# Molecular Design and Preparation of Protein-based Soft Ionic Conductors with Tunable Properties

Xin Yu,<sup>1,§</sup> Yang Hu, <sup>1,§</sup> Haoyuan Shi,<sup>2,§</sup> Ziyang Sun, <sup>1</sup> Jinghang Li, <sup>1</sup> Haoran Liu, <sup>1</sup> Hao Lyu, <sup>1</sup> Jiujie Xia, <sup>1</sup> Jingda Meng, <sup>1</sup> Ruochuan Huang, <sup>1</sup> Xingyu Lu,<sup>3</sup> Jingjie Yeo,<sup>2,\*</sup> Qiyang Lu,<sup>1,4\*</sup> Chengchen Guo<sup>1,\*</sup>

- 1. School of Engineering, Westlake University, Hangzhou 310024, China
- Sibley School of Mechanical and Aerospace Engineering, Cornell University, Ithaca, NY 14853, USA
- Key Laboratory of Precise Synthesis of Functional Molecules of Zhejiang Province, Instrumentation and Service Centre for Molecular Sciences, Westlake University, Hangzhou 310024, China
- Key Laboratory of 3D Micro/Nano Fabrication and Characterization of Zhejiang Province, Westlake University, Hangzhou 310024, China
- § These authors contributed equally

**ABSTRACT** 

Protein-based soft ionic conductors have attracted considerable research interest in recent years

with great potential in applications at the human-machine interfaces. However, a fundamental

mechanistic understanding of the ionic conductivity of silk-based ionic conductors is still

unclear. Here, we first developed an environmental-friendly and scalable method to fabricate

silk-based soft ionic conductors using silk proteins and calcium chloride. The mechanistic

understanding of the ion transport and molecular interactions between calcium ions and silk

proteins at variable water contents were investigated in-depth by combining experimental and

simulation approaches. The results show that the calcium ions primarily interact with amide

groups in proteins at a low water content. The ionic conductivity is low since the calcium ions

are confined around silk proteins within 2.0~2.6 Å. As water content increases, the calcium

ions are hydrated with the formation of water shells, leading to the increased distance between

calcium ions and silk proteins (3.3~6.0 Å). As a result, the motion of the calcium ions increased

to achieve a higher ionic conductivity. By optimizing the ratio of the silk proteins, calcium ions,

and water, silk-based soft ionic conductors with good stretchability and self-healing properties

can be obtained. Such protein-based soft ionic conductors can be further used to fabricate smart

devices such as electrochromic devices.

KEYWORDS: Silk protein, soft ionic conductors, structure-properties relationships, protein-

ion interaction, ionic conduction mechanism

2

#### INTRODUCTION

Natural living systems conduct signals and regulate physiological activities mainly using ions, which inspires scientists to develop bio-inspired soft ionic conductors for flexible epidermal electronics or for integrating humans and machines.<sup>1-4</sup> Soft ionic conductors typically contain three main components of polymer, ions, and water, while elastomer-based soft ionic conductors do not contain water.<sup>5, 6</sup> The polymer forms the network and provides structural support. The ions released from dissolving salt in water enhance the conductivity of the hydrogel depending on the type and the concentration of the salt.<sup>1,7</sup> Over the past a few years, a variety of material systems have been reported for constructing soft ionic conductors, such as polyacrylamide (PAAm)/sodium chloride/water,<sup>3</sup> (PAAm)/lithium chloride/water,<sup>8, 9</sup> poly(vinyl alcohol) /borax,10 and silk proteins/calcium chloride/water.11,12 Among all these systems, soft ionic conductors made from silk proteins attracted scientific scrutiny since they mimic natural biological systems very well as proteins (a class of biopolymers) are usually used to form the polymer networks. <sup>13, 14</sup> Silk proteins are naturally occurring biopolymers commonly extracted from cocoons. They have recently been used widely to make biocompatible proteinbased flexible electronic devices such as epidermal sensors. [15-21] Besides biocompatibility, silk proteins possess other appealing features, including biodegradability, eco-friendly processing, and tunable mechanical properties.<sup>22, 23</sup> In reported silk protein-based soft ionic conductors, calcium chloride (CaCl<sub>2</sub>) was commonly employed as the dispersed salt in the system, releasing ions for conducting electricity. 12, 24-26 Previous studies have shown proofs of concept for the use of silk proteins/CaCl<sub>2</sub> ionic conductors (termed Silk-Ca ICs) to create soft electronic devices and artificial skins with sensory capabilities. 11, 12, 24, 27 Recently, Ling and co-workers investigated the influence of hydrated protons on temperature and humidity responsiveness of Silk-Ca ICs.<sup>28</sup> However, a clear mechanistic understanding of ion transport and molecular interactions between calcium ions and silk proteins are still lacking. In addition, a green and

scalable processing method is also needed to fabricate Silk-Ca ICs with tailored physical properties and biocompatibility.

In this study, we develop a green approach with potential of scale-up production to prepare Silk-Ca ICs using silk proteins derived from natural cocoons and calcium chloride. We investigate the Silk-Ca ICs thoroughly by combining advanced experimental characterization techniques and molecular dynamics (MD) simulations. We focus on elucidating the dynamic interactions between protein chains and ions at different water contents and revealing the structure-properties relationships in Silk-Ca ICs. We also demonstrate that the Silk-Ca ICs have tunable conductivity, self-healing properties, and good stretchability, which allows the fabrication of smart devices such as electrochromic devices. The silk-based ICs show great potential in developing implantable ionic conductors at the human-machine interfaces.

#### RESULTS AND DISCUSSION

Silk-Ca ICs with tunable conductivity and physical properties were prepared using silk proteins derived from natural cocoons and CaCl<sub>2</sub> (Figure 1). Briefly, silk solution (5.0 w/v%) and CaCl<sub>2</sub> solution (1.0 M) were mixed at specific weight ratios and freeze-dried to obtain Silk-Ca powder. The powder samples are annotated as Silk-Ca-X where X refers to the weight ratio of silk to CaCl<sub>2</sub>. [Silk-Ca-0.5; Silk-Ca-1; Silk-Ca-2] The Silk-Ca powder was then mixed with pure water homogeneously to prepare Silk-Ca ICs. By tuning the amount of water in the system, the physical state of Silk-Ca ICs can be tuned from gel state to viscous solution as indicated by rheology results (Figure S1). Briefly, the complex viscosity and modulus of Silk-Ca ICs decreased significantly with the increase of water content. Furthermore, the ionic conductivity of the Silk-Ca ICs can be tuned and shows strong correlations with the water content and the ratios of silk to CaCl<sub>2</sub>. A detailed mechanistic study combining advanced experimental

characterizations and molecular dynamics (MD) simulation was carried out in this work to elucidate the "structure-properties" relationships of the Silk-Ca ICs.

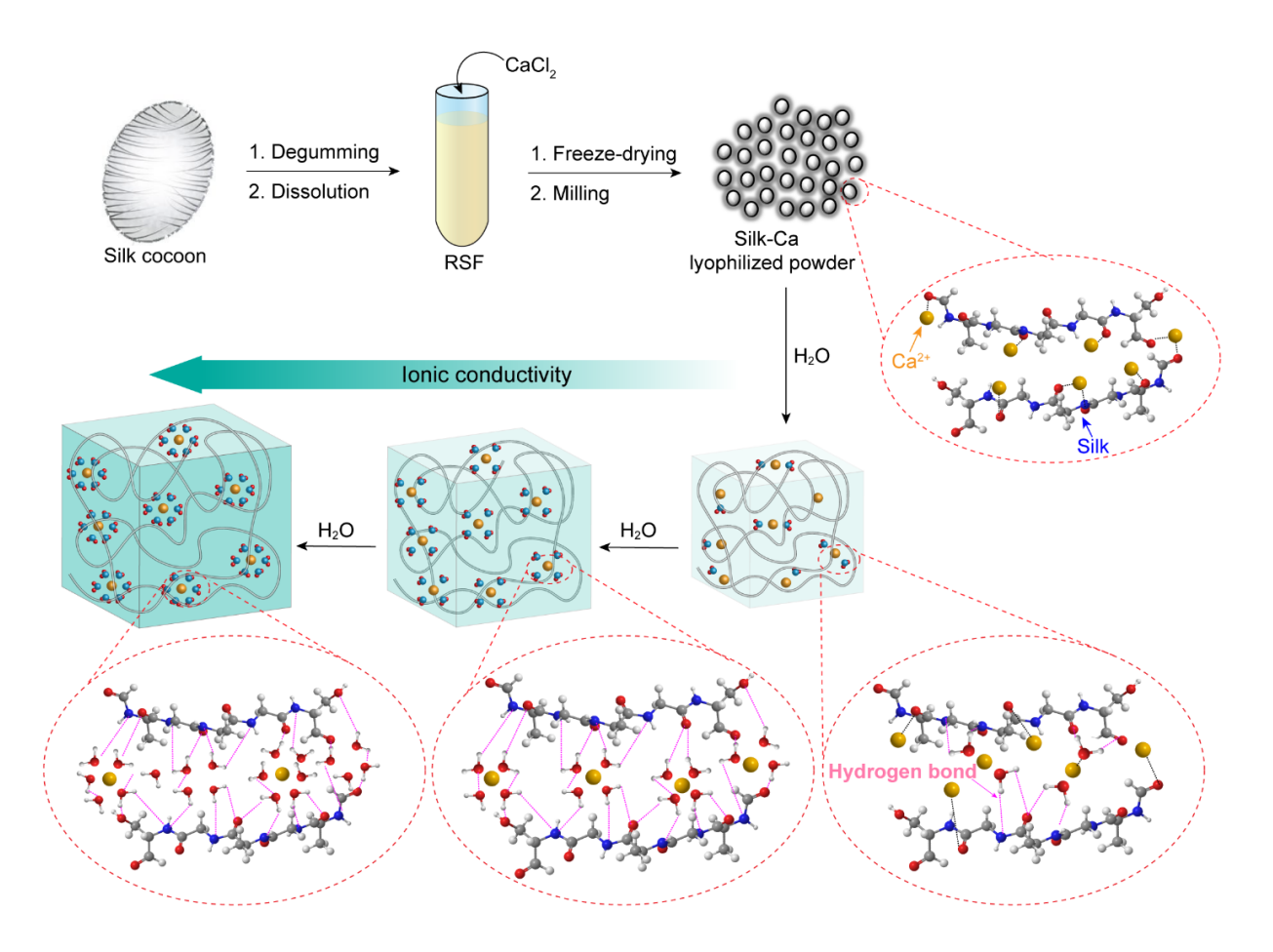
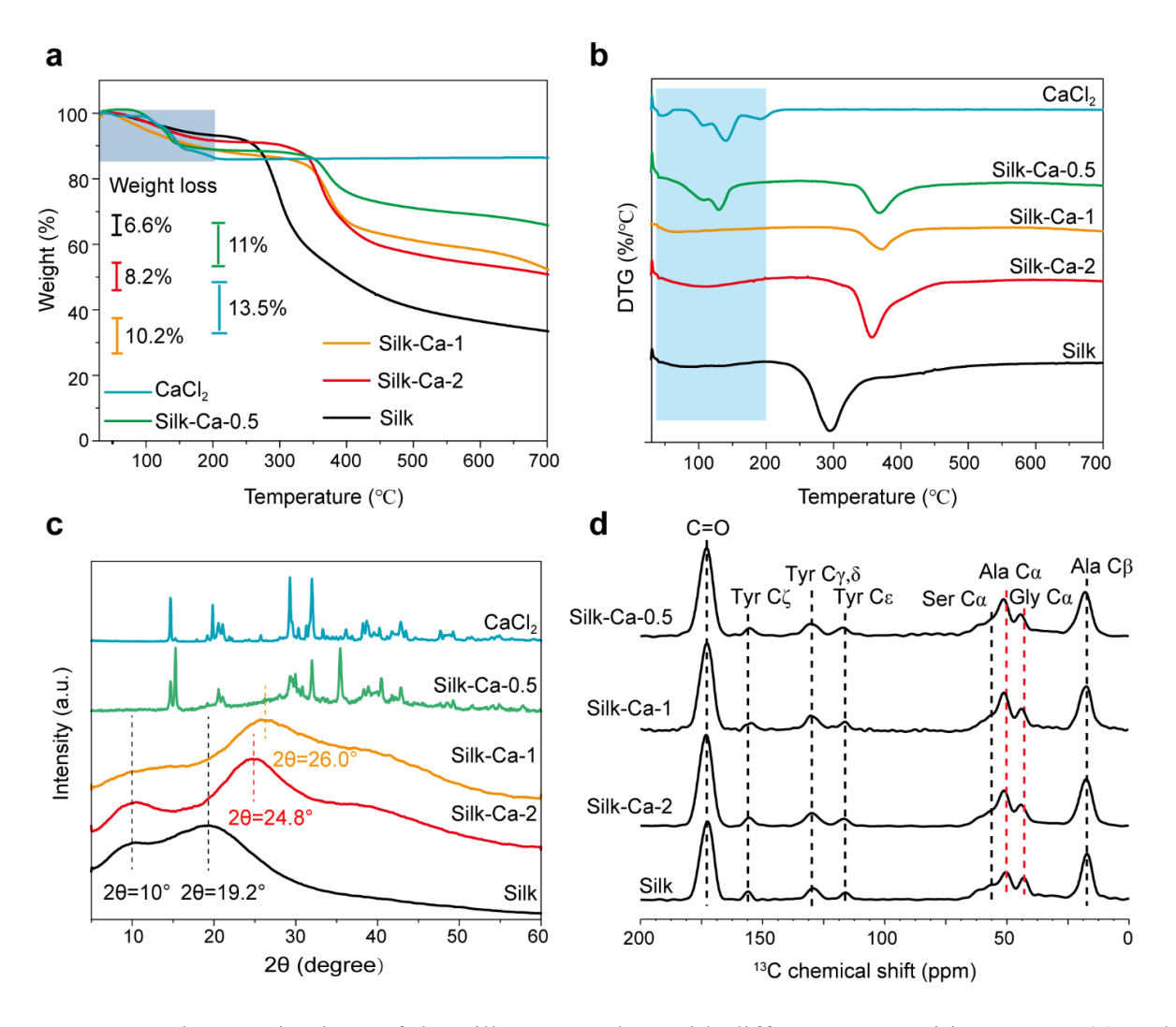


Figure 1. Schematic illustration of preparation of Silk-Ca ICs with tunable properties.

Figure 2a shows the TGA profiles of Silk-Ca powders with different ratios of silk to CaCl<sub>2</sub>. Compared to pure silk, the Silk-Ca powder with a higher content of CaCl<sub>2</sub> shows a smaller weight loss upon heating up to 700 °C due to the high stability of CaCl<sub>2</sub>. However, the ratio of weight loss below 200 °C (blue region) increased from 6.6 % to 13.5 % as the CaCl<sub>2</sub> content increased. The weight loss below 200 °C is attributed to the amount of water in the sample, including both free water and bound water. Due to the strong water-binding capacity of CaCl<sub>2</sub>, the Silk-Ca powder with a higher content of CaCl<sub>2</sub> can bind to more water molecules, resulting in a greater weight loss below 200 °C. Furthermore, the DTG curve of the Silk-Ca-0.5 powder indicates that excessive bulk CaCl<sub>2</sub> is present in the system (highlighted in blue, Figure 2b).



**Figure 2.** Characterizations of the Silk-Ca powders with different compositions. TGA (a) and DTG (b) curves of the Silk-Ca powders with different ratios of silk to CaCl<sub>2</sub>. c. XRD profiles of the Silk-Ca powders with different ratios of silk to CaCl<sub>2</sub>. d. Solid-state <sup>13</sup>C NMR spectra of the Silk-Ca powders with different ratios of silk to CaCl<sub>2</sub>.

However, for Silk-Ca-1 and Silk-Ca-2 powders, no bulk CaCl<sub>2</sub> was observed, and all Ca<sup>2+</sup> was bound to silk proteins. This result agrees well with the DSC results, where the Silk-Ca-0.5 powder showed fluctuating water desorption over 150 °C (Figure S2). In addition, the thermal degradation temperature of the silk increased in the Silk-Ca powders compared with pure silk, indicating that the introduction of CaCl<sub>2</sub> promoted the thermal stability of the silk due to Silk-Ca<sup>2+</sup> interactions. As shown in Figure 2c, the XRD pattern of pure silk powders has two broad peaks centered at 10° and 19.2°, indicating pure silk powders were amorphous. Regarding Silk-Ca-1 and Silk-Ca-2 powders, the XRD patterns showed amorphous structures with two broad peaks. Compared with pure silk, the broad peak at 19.2° shifted to 24.8° and 26.0° for Silk-Ca-

2 and Silk-Ca-1 powders, respectively. The results indicated that calcium ions interact strongly with the silk proteins while the amorphous structure of silk proteins was not influenced dramatically. The XRD patterns of the Silk-Ca-0.5 showed characteristic peaks of crystalline CaCl<sub>2</sub>, indicating the existence of excessive bulk CaCl<sub>2</sub>. ATR-FTIR spectroscopy also showed that introducing CaCl<sub>2</sub> did not significantly affect the amorphous structures of silk proteins. At the same time, the presence of CaCl<sub>2</sub> associated water peaks indicated the presence of excessive bulk CaCl<sub>2</sub> when the ratio of silk to CaCl<sub>2</sub> increased to 2 (Figure S3). To elucidate the molecular interactions between Ca<sup>2+</sup> and silk proteins, solid-state NMR spectroscopy was applied. From the <sup>13</sup>C cross-polarization magic-angle-spinning (CP-MAS) NMR spectra of pure silk and Silk-Ca powders (Figure 2d), it is found that the resonance of Ala C<sub>β</sub> presented at 17 ppm in all samples, indicating the alanine residues in silk proteins were primarily in random coil or helical structures.<sup>29</sup> However, with increasing CaCl<sub>2</sub> content in the Silk-Ca powders, the resonances of the Gly  $C_{\alpha}$  and Ala  $C_{\alpha}$  showed slight shifts, which is likely due to the strong interactions between Ca<sup>2+</sup> and amide groups in proteins (Figure S4). The NMR results indicate that Ca<sup>2+</sup> not only interacts with carboxyl groups (e.g., aspartic acid and glutamic acid) but also with the amide groups in silk proteins.<sup>[24]</sup>

Based on the structural characterizations of the Silk-Ca powders, we then choose Silk-Ca-1 and Silk-Ca-2 powders to prepare the Silk-Ca ICs since no excessive bulk CaCl<sub>2</sub> was observed in these two samples. The morphologies of these two powder samples were characterized by SEM, showing the powders are composed of microparticles (Figure S5). The Silk-Ca ICs were obtained by mixing the Silk-Ca powder with a specific amount of pure water. The ionic conductivities of Silk-Ca ICs with different water contents were characterized by electrochemical impedance spectroscopy (EIS) (Figure 3a). The equivalent circuit for the EIS measurement was shown in Figure S6. All EIS Nyquist plots had linear trends (Figure 3b, Figure S7 and Figure S8), indicating that the ionic conduction within the Silk-Ca ICs at different

water contents is a non-Faradaic process where no matter or charge crossed the electrodeconductor interface.<sup>30</sup>

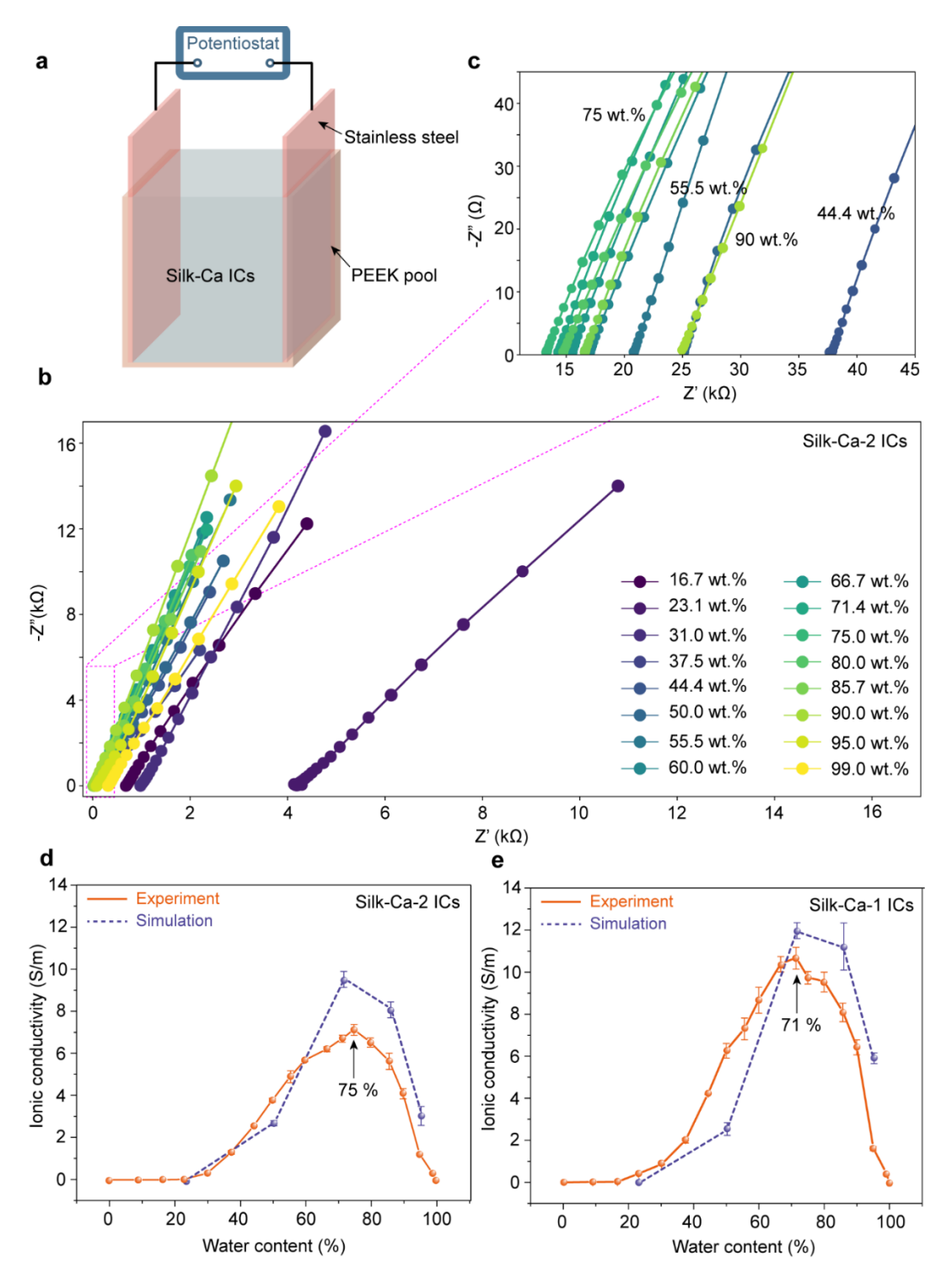


**Figure 3.** Ionic conductivity of Silk-Ca ICs. a. Schematic illustration of ionic conductivity measurements via electrochemical impedance spectroscopy (EIS). b-c. EIS Nyquist plot of Silk-Ca-2 ICs at different water contents (b:16.7 wt%  $\sim$  99 wt%, c: zoomed in, 44.4 wt%  $\sim$  90 wt%). d-e. Ionic conductivity of Silk-Ca ICs from experiment (line) and simulation (dot) plotted as a function of the water content.

In addition, the impedance of Silk-Ca-2 ICs, measured from the intercepts of the EIS Nyquist curves with the x-axis, decreased with increasing water content initially. The impedance reached a minimum at a water content of 75 wt%, then increased subsequently as water content further increased to 99 wt% (Figure 3c). For Silk-Ca-1 ICs, a similar trend was observed (Figure S6). The ionic conductivity of Silk-Ca ICs derived from the impedance (Figure 3d, 3e) was compared to the impendence and ionic conductivity of CaCl<sub>2</sub> solutions at different water contents (Figure S8 and Figure S9). The ionic conductivity of samples with or without silk showed similar trends as the water content increased. Specifically, at a low water content, the ionic conductivity was low. As the water content increased, the ionic conductivity increased gradually and reached maximum at moderate water content and then decreased to almost zero in the end. At the maximum ionic conductivity, it was found that Silk-Ca-2 IC (~75 wt%.) had higher optimal water content than Silk-Ca-1 IC (~71 wt%.) while Silk-Ca-1 ICs showed higher ionic conductivity than Silk-Ca-2 ICs at same water content. This behavior may be caused by the tortuous network formed by silk proteins, which inhibits the movement of ions. Apart from the experiment, the ionic conductivity of Silk-Ca ICs was also calculated using the Nernst-Einstein equation in MD simulation, which agreed well with the experimental results (Figure 3d and 3e).

To elucidate the mechanism of ionic conduction at the molecular level and reveal the "structure-properties" relationship in Silk-Ca ICs, solid-state <sup>1</sup>H magic angle spinning (MAS) radio frequency-driven recoupling (RFDR) NMR spectroscopy was applied to probe the interactions between silk proteins, Ca<sup>2+</sup>, and water. From Figure 4a, the resonance of water showed upfield shifts with increasing the water content, indicating that the water molecules were confined at a low water content and became more dynamic at a high water content. Similarly, the resonances of silk proteins in the Silk-Ca-2 and Silk-Ca-1 became sharper with increasing water content, indicating the increasing mobility of silk proteins (Figure 4b). Furthermore, the resonances of NH and Ser-OH groups in silk proteins showed upfield shifts

(red and blue dotted lines) as the water content increased, which is attributed to the formed hydrogen bonding between hydrated Ca<sup>2+</sup> and amide/Ser-OH groups. For other groups (black dotted lines) in Ala, Tyr, and Gly residues, the resonances did not change with increasing the water content. 2D solid-state <sup>1</sup>H-<sup>1</sup>H MAS RFDR NMR spectroscopy was further applied to probe the molecular interactions in the sample of Silk-Ca-2 with a water content of 50 wt%. As shown in Figure 4c, the resonances of NH and Gly/Ala CHα and Ala CHβ of silk proteins show interaction with water molecules at a short mixing time (0.5 ms), indicating water molecules are close to these groups. At a longer mixing time (5 ms), the Ser-OH showed interaction with the water, indicating the distance between Ser-OH group and water molecules is relatively longer.

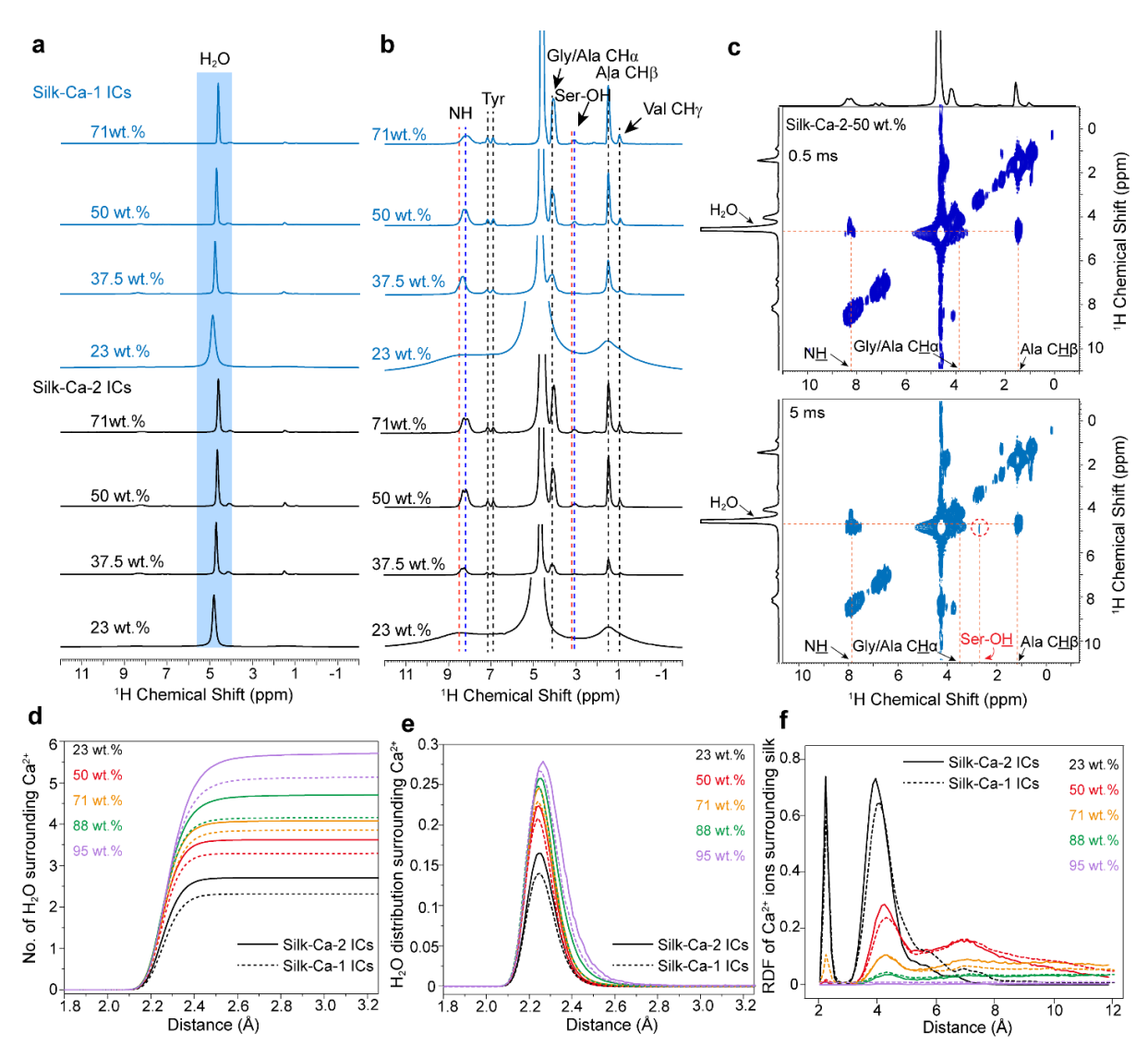


**Figure 4.** a, b. Solid-state <sup>1</sup>H MAS RFDR NMR spectra of Silk-Ca ICs at different water contents. c. 2D <sup>1</sup>H-<sup>1</sup>H MAS RFDR NMR spectra of the Silk-Ca-2 IC containing 50 wt%. of water content at mixing times of 0.5 ms and 5 ms, respectively. d. The average number of water molecules surrounding each Ca<sup>2+</sup> ion in Silk-Ca ICs. e. The distribution of water molecules surrounding each Ca<sup>2+</sup> ion in Silk-Ca ICs. f. The radial distribution function (RDF) of Ca<sup>2+</sup> surrounding silk proteins in Silk-Ca ICs.

MD simulations were also carried out to reveal the mechanism of ionic conduction. Briefly, the representative silk protein with amorphous structures was obtained using replica exchange molecular dynamics (REMD) simulations<sup>31</sup> with global exchange of replicas (TIGER2).<sup>32</sup> In the MD simulation, the diffusion coefficient of Ca<sup>2+</sup> was determined by fitting a linear model to the particle-averaged mean squared displacement (MSD) function with time (Figure S10 and Table S1). The results showed that the diffusion coefficient of Ca<sup>2+</sup> increased with the increase of the water content. Since the ionic conductivity and the mobility of the Ca<sup>2+</sup> are intimately related to the water content within each system, we calculated the positional relationship between Ca<sup>2+</sup> and water molecules. In the Silk-Ca systems, increasing the water content significantly hydrated the Ca2+ with more water molecules in their immediate surroundings (Figure 4d). The distribution of the water molecules (Figure 4e) showed that the water molecules mainly resided between 2.1 to 2.6 Å away from the Ca<sup>2+</sup>, forming a water shell. This insight supports the results obtained from both experiments and simulations that the diffusion coefficient and the mobility of Ca<sup>2+</sup> increased as the water content increased. Furthermore, by comparing the distribution curves of water molecules for Silk-Ca-2 and Silk-Ca-1, the hydration of Ca<sup>2+</sup> was not saturated when the water content was below 90 wt%., which explained the increasing diffusion coefficient of Ca<sup>2+</sup> in Silk-Ca systems as the water content increased (Table S1). Besides, Silk-Ca-2 had a larger magnitude of the diffusion coefficient than Silk-Ca-1 at the same water content since fewer numbers of Ca<sup>2+</sup> in Silk-Ca-2 resulted in more hydrated Ca<sup>2+</sup>, thereby showing greater mobility. Other than diffusion coefficient, the number density of ions was another factor that affects ionic conductivity. Thus, even if the diffusion coefficient was higher in Silk-Ca-2, the competing effect of a much lower number density of ions in the system resulted in a lower ionic conductivity than Silk-Ca-1 at the same water content. This reason can also explain the decreased ionic conductivity: as the water content continued to increase, the increase in diffusion coefficient was not as fast as the decrease in the number density of ions due to the almost saturated hydration of the ions.

Besides the relative positional relationship between water molecules and Ca<sup>2+,</sup> in-depth insight into the distribution of Ca<sup>2+</sup> around silk proteins and the locations of silk-Ca<sup>2+</sup> binding sites are also needed for achieving a better material design and property tuning of Silk-Ca ICs. MD simulation results indicated that the Silk-Ca ICs with a lower water content led to a larger number of Ca<sup>2+</sup> localizing around silk proteins due to the strong silk-Ca<sup>2+</sup> interactions and the confined space for ionic motion (Figure S11). Moreover, there were two distinct peaks for the Silk-Ca ICs with a water content of 23 wt%, but both gradually diminished in tandem with increasing water content (Figure 4f). Since the RDF curves were time-averaged for each case, the peak could be attributed to two situations: 1) Ca<sup>2+</sup> that was rigidly bound to proteins at specific distances; 2) Ca<sup>2+</sup> that diffused around, hopping in and out within those narrow intervals. The first peak at a distance of 2.0 to 2.6 Å was attributed to the rigidly bound Ca<sup>2+</sup> due to the strong silk-Ca<sup>2+</sup> interactions, where Ca<sup>2+</sup> mainly interacted with the amide groups and the hydroxyl groups of the Ser residues (Table S2 and Figure 3a-3c). However, as the water content increased, the first peak in the RDF profiles decayed dramatically, indicating fewer direct silk-Ca<sup>2+</sup> interactions led to broadened distance distributions between Ca<sup>2+</sup> and silk proteins. Introducing more water into the system would break the interactions between the Ca<sup>2+</sup> and the silk protein, where the Ca<sup>2+</sup> primarily interacts with the water molecules instead of the silk proteins to form more hydrated Ca<sup>2+</sup>. Nevertheless, the water molecules around the hydrated Ca<sup>2+</sup> could still form hydrogen bonds with the amide groups and hydroxyl groups in silk proteins, contributing to the second peak at a distance of 3.0 to 6.0 Å. At this stage, Ca<sup>2+</sup> was fluidized by water molecules, hopping in and out within this interval since no rigidly bound calcium ions were detected. At a higher water content, the silk-Ca<sup>2+</sup> interactions weakened because the Ca<sup>2+</sup> were fully hydrated, hence the second RDF peak gradually diminished as water content increased. This also explained why the peak values of the RDF curves in Silk-Ca-2 and Silk-Ca-1 became closer as water content increased since the number of binding sites in silk was no longer a limiting factor.

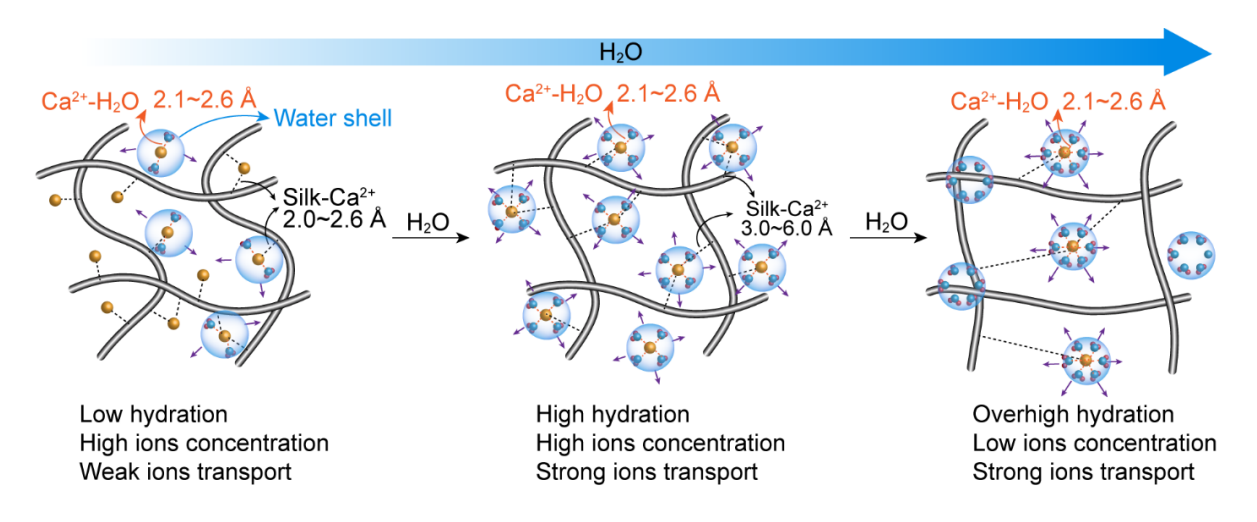


**Figure 5.** Schematic illustration of ionic conduction mechanism of Silk-Ca ICs with varying water contents.

Combining the experimental findings and simulation results, a clear mechanistic understanding of the ionic conduction in the Silk-Ca ICs was achieved and summarized in Figure 5. At low water content, only a small number of Ca<sup>2+</sup> are hydrated due to the strong water absorption capacity of Ca<sup>2+</sup>, while the majority of dissociated Ca<sup>2+</sup> close to the silk backbone (2.0~2.6 Å) are confined and unable to transport due to the strong interactions between the entangled silk polymer network and Ca<sup>2+</sup>. Thus, Silk-Ca ICs with low water content show negligible conducting performance. By introducing more water, more Ca<sup>2+</sup> are hydrated where these ions interact with silk proteins (3.0~6.0 Å) via hydrogen bonding between water molecules in the hydrated shell and the amide or hydroxyl groups in the silk proteins. The hydration of Ca<sup>2+</sup> significantly enhanced the mobility and transport of Ca<sup>2+</sup> in the Silk-ICs. Consequently, the ionic conductivity of the Silk-ICs increased and peaked at a moderate water content. Thereafter, increasing water content not only suppresses the silk-Ca<sup>2+</sup> interaction by

conferring much higher mobility to Ca<sup>2+</sup> in the system but also reduces the ion concentration due to the free water molecules, which leads to decreased ionic conductivity.

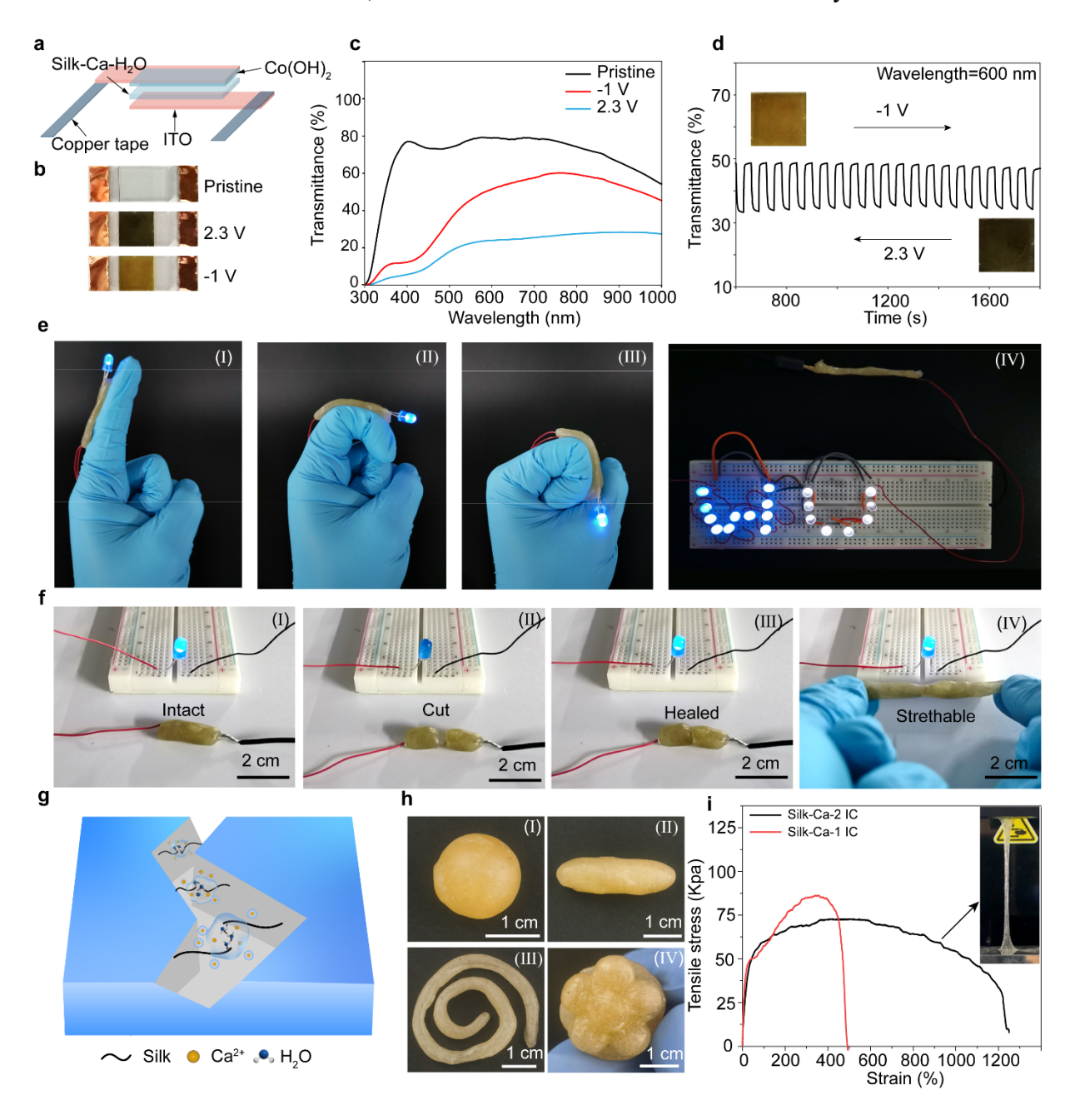


**Figure 6.** Demonstration and applications of Silk-Ca ICs. a. Schematic illustration of electrochromic device fabrication by using Silk-Ca IC (water content ~ 60 wt%) as electrolyte. The Silk-Ca IC was prepared using Silk-Ca-1 with a water content of 60 wt%. b. Digital images of electrochromic devices before and after positive and negative voltage supply. c. Transmittance spectra of electrochromic devices at different states. d. Transmittance-time curve of the electrochromic devices at stepping potential (2.3 V and -1 V for 30 s) with a wavelength of 600 nm. e. Demonstration of Silk-Ca ICs on hand (I: up, II: level, III: down) with DC applied to maintain current and illuminating LED (acronym of Westlake University) by using Silk-Ca ICs as conductive wire (IV). f. Self-healing performance of Silk-Ca ICs in electronic circuit (I: intact, II: cut, III: healed, IV: stretchable). g. Illustration of self-healing mechanism. h. Shape flexibility of Silk-Ca ICs (I: ball, II: rod, III: strip, IV: flower). i. Tensile stress-strain curves

of the Silk-Ca ICs. The Silk-Ca ICs in (e-i) was prepared using Silk-Ca-2 with a water content of 23 wt%.

The Silk-Ca ICs can be used to fabricate advanced electronic devices. In this study, an electrochromic device was fabricated using Silk-Ca IC, ITO, and Co(OH)<sub>2</sub> coated ITO as the electrolyte, transparent conducting oxide, and electrochromic layer/transparent conducting glass, respectively (Figure 6a). The Silk-Ca IC was prepared using Silk-Ca-1 with a water content of 60 wt%. The pristine device is transparent, while the color became dark brown after positive voltage supply, and the color turned to dark yellow when the voltage shifted to negative (Figure 6b). The transmittance of the electrochromic device at different states was shown in Figure 6c, and the value was consistent with their corresponding color. The transmittance of the electrochromic device at different states decreased in the order of pristine > -1.0 V > 2.3 V. Transmittance-time plots showed that highly reversible color change shifted from dark brown with low transmittance to dark yellow with relative high transmittance under positive and negative potential, respectively (Figure 6d). The ionic conductivity of the Silk-Ca ICs was further demonstrated by serving as a conductor in a circuit to light a high-emitting diode (LED) using an 8 V DC power source. As shown in Figure 6e, the Silk-Ca IC was prepared using Silk-Ca-2 with a water content of 23 wt%. Negligible changes in the light brightness could be observed during finger movement (I: up, II: level, III: down), indicating the Silk-Ca IC was able to continuously transmit a steady DC electronic signal regardless of mechanical deformations. In addition, the Silk-Ca IC can also transmit steady electricity to light multiple LEDs ("WU": acronym of Westlake University). Furthermore, this Silk-Ca IC has self-healing properties. Once the Silk-Ca IC was cut into two pieces using a razor blade, the LED photoemission stopped consequently (Figure 6f). However, when the two separated pieces were placed together, the interface rapidly healed to restore the electrical conduction and stretchability without applying heat or moisture stimuli. The self-healing properties are attributed to the dynamic hydrogen binding between hydrated Ca<sup>2+</sup> and silk proteins, as illustrated in Figure 6g.

The Silk-Ca ICs could also be molded into complex shapes, such as balls, rods, strips, and flowers (Figure 6h). Figure 6i shows the stress-strain curve of the Silk-Ca IC. The results indicated that the Silk-Ca-2 IC could be stretched over 1000%, showing the great potential of silk-based ionic conductors in stretchable electronics.

### **CONCLUSION**

In this study, we developed a green and scalable method to construct silk-based soft ionic conductors based on silk proteins, calcium chloride, and water. Both experimental and simulation results indicate that dynamic interactions between protein chains and ions at different water contents allow the tunability of the ionic conductivity. The calcium ions primarily interact with amide groups in proteins at low water content. The ionic conductivity is low since the calcium ions are confined around silk proteins within 2.0~2.6 Å. As water content increases, the calcium ions are hydrated with the formation of water shells, leading to the increased distance between calcium ions and silk proteins (3.3~6.0 Å). As a result, the dynamic of the calcium ions increased to achieve a higher ionic conductivity. After reaching the maximum ionic conductivity at a moderate water content, the ionic conductivity decreases gradually due to the excessive water reducing the density of hydrated calcium ions. Additionally, silk-based soft ionic conductors with good stretchability and self-healing properties can be obtained by optimizing the composition of silk proteins, calcium ions, and water. Such proteinbased soft ionic conductors can be further used to fabricate smart devices such as electrochromic devices. Overall, this study provides a fundamental understanding of the structure-properties relationships for protein-based soft ionic conductors and insights into novel materials design at the human-machine interfaces.

## **Experimental Section/Methods**

Materials. Bombyx mori (B. mori) silkworm cocoons were supplied by local manufacturer. Anhydrous sodium carbonate (Na<sub>2</sub>CO<sub>3</sub>, 99%), lithium bromide (LiBr, 99%), anhydrous

calcium chloride (CaCl<sub>2</sub>, 99%) were purchased from Aladdin and used as received. Deionized (DI) water (18 M $\Omega$ ) produced with a Milli-Q system was used in the study.

Preparation of regenerated silk solution. B. mori silkworm cocoons were cut into small pieces and washed with DI water. The cleaned cocoon pieces were boiled in a solution of Na<sub>2</sub>CO<sub>3</sub> (0.02 M) for 30 min to remove the sericin. This process refers to degumming. The degummed silk was washed with DI water to remove the Na<sub>2</sub>CO<sub>3</sub> and sericin, followed by drying at ambient condition overnight. The dried degummed silk was then dissolved in the 9.3 M LiBr aqueous solution at 60 °C for 4 h (Silk/LiBr solution=20% wt/vol). The silk solution was dialyzed against DI water for 3 days using Slide-a-Lyzer dialysis cassettes (MWCO 3,500, Pierce). After dialysis, the solution was purified by centrifugation for 20 min at 9000g twice. The concentration of the purified silk solution was determined by drying 1.0 mL of the solution and measuring the dried silk. The concentration of the purified silk solution is about 6 w./v.%. The molecular weight of purified silk fibroin was estimated via gel electrophoresis and it is about 140 kDa (Figure S12).

Preparation of Ca<sup>2+</sup> modified silk (Silk-Ca) powders. An aqueous solution of CaCl<sub>2</sub> (1.0 M) was made and added into silk solution (5 wt%.) at specific mass ratios of silk to CaCl<sub>2</sub> (Silk/CaCl<sub>2</sub> = 2:1, 1:1, and 1:2, denoted as Silk-Ca-2, Silk-Ca-1, and Silk-Ca-0.5, respectively). The Silk-Ca solution was frozen with liquid N2, followed by lyophilization at -50 °C and 0.02 bar. The lyophilized Silk-Ca sponges were then milled into ultrafine powders using a high-speed miller (IKA, Germany), producing the product referred to Silk-Ca powders. The Silk-Ca powders were stored at dry conditions to prevent any rehydration until used in the following steps.

**Preparation of Silk-Ca Ics.** The Silk-Ca ICs were prepared by mixing the Silk-Ca powder with water and incubation at 60 °C for 24 h with gentle stirring. Silk-Ca ICs with various water contents were defined as Silk-Ca-x-y gel, where x and y represent the ratio of silk to CaCl<sub>2</sub> and water content (wt%.), respectively. When water content is over 1, the Silk-Ca viscous solution

was obtained instead of gel. When water content is further increased to 3 or more, the Silk-Ca dilute solution was obtained. Table 1 shows the compositions of Silk-Ca ICs used Silk-Ca-2 as example. The other Silk-Ca ICs used Silk-Ca-1 and Silk-Ca-0.5 are same to Silk-Ca-2.

Table 1. The compositions of Silk-Ca ICs used Silk-Ca-2 as solid powder

Silk-Ca-2	$H_2O$	Symbol	State
1 g	0.1 g	Silk-Ca-2-9.1 wt%.	Heterogenous
1 g	0.3 g	Silk-Ca-2-23.1 wt%.	Gel
1 g	1 g	Silk-Ca-2-50 wt%.	Viscous solution
1 g	9 g	Silk-Ca-2-90 wt%.	Dilute solution

Ionic conductivity. The ionic conductivity of Silk-Ca ICs at different water contents were calculated from the corresponding Nyquist plots measured using the AC impedance technique. The samples were packed completely into a cell with 1 cm in length, 1 cm in width, and 1 cm in height and subjected to connect with potentiostat (Admiral Squidstat Plus) via conductive stainless-steel electrode. The Nyquist plots of sample were conducted by performing electrochemical impedance spectroscopy (EIS) with 20 mV amplitude at open-circuit-voltage (OCV). The measurements were performed in the frequency of 100 kHz to 1 Hz under a standard lab condition (25 °C and 50% RH). The intersection of the Nyquist plots at the real part was considered as the bulk resistance of the Silk-Ca ICs electrolyte (Rb), and the ionic conductivity can be obtained from the following equation:

$$\sigma = \frac{L}{R_h \times A}$$

where L is the length of the electrolyte and A is the electrode area.

NMR spectroscopy. Solid-state NMR spectroscopy was used to characterize the molecular structures of silk proteins and the interaction between silk and Ca<sup>2+</sup> and water in the prepared Silk-Ca ICs. The NMR experiments were performed on a Bruker 500 MHz spectrometer (Bruker, Germany) equipped with a 3.2 mm triple resonance probe ( ${}^{1}H/{}^{13}C/{}^{15}N$ ). Sample was loaded in a standard zirconia rotor with Torlon cap for each measurement.  ${}^{1}H \rightarrow {}^{13}C$  crosspolarization magic angle spinning (CP-MAS) NMR spectra were obtained with the CP condition of a 2.3  $\mu$ s  ${}^{1}H \pi/2$  pulse with a power level of 60 W, followed by a 2.0 ms contact

time at 30 W power. The experiments were conducted at 2.0 s recycle delay, 50 kHz sweep width, 20,480 scans, and the magic angle spinning speed of 20 kHz for all samples. Solid-state 2D  $^{1}$ H/ $^{1}$ H radio frequency-driven recoupling (RFDR) under magic-angle-spinning (MAS) was recorded at 5.0  $\mu$ s  $^{1}$ H  $\pi$ /2 pulse followed by 10.0  $\mu$ s  $^{1}$ H  $\pi$  pulse with a power level of 60 W. The experiments were performed at 2.0 s recycle delay, 16 time. The cross-polarization (CP) and 2D  $^{1}$ H/ $^{1}$ H RFDR-MAS experiments were performed at a spinning speed of 20 kHz. Tetramethylsilane (TMS) was used as a reference.

Thermo analysis. The thermal stability of the Silk-Ca powders was characterized by thermogravimetric analysis (TGA), where the sample was heated from 30 °C to 800 °C in N<sub>2</sub> at a heating rate of 10 °C min<sup>-1</sup>. For all measurements, samples were kept under N<sub>2</sub> in the furnace to reach a stable weight prior to heating. DSC measurements were carried out on a Mettler Toledo instruments DSC3 calorimeter under a dry N<sub>2</sub> gas flow of 50 ml min<sup>-1</sup>. In standard DSC measurements, approximately 5 mg of Silk-Ca powders encapsulated in aluminum pans were heated from ambient temperature to 230 °C with a scanning speed of 10 °C min<sup>-1</sup>. Multiples cycles (n>=3) were performed on each sample to ensure the data reproducibility.

**X-Ray diffraction.** The X-Ray diffraction (XRD) analysis was performed on the Bruker D8 Advance (Germany) instrument using Cu Kα radiation. The wavelength of the X-Ray beam was 1.5418 Å with a fixed energy of 8.04 keV and the irradiation voltage and current were 40 kV and 40 mA respectively. The XRD patterns were collected in the 2θ range of 5-60° with a scanning speed of 3° min<sup>-1</sup>.

**Scanning electron microscopy.** Surface morphology was observed on the Zeiss Gemini 450 (Germany) scanning electron microscopy (SEM) operated at an acceleration voltage of 3 kV. Energy dispersive X-Ray (EDX) analysis was undertaken on Gemini 450 with integrated EDX detector.

**Rheology.** Rheological characterization was recorded on an advanced rotational rheometer (ARES-G2, TA-Waters, USA) equipped with a 25 mm parallel plate geometry. Small amplitude

oscillatory shear measurements were performed from 100 to 0.01 rad s<sup>-1</sup> at a low strain of 1%, which is within the linear viscoelastic regime. Flow sweep experiments were performed from 0.1 to 100 s<sup>-1</sup>. All experiments were carried out at a gap of 0.5 mm under a standard lab condition  $(25\pm1 \, ^{\circ}\text{C}, 50\pm5\% \, \text{RH})$ .

Mechanical properties tests. The tensile tests of Silk-Ca ICs were carried out on a CellScale Biomaterials Testing system (CellScale Inc.) at 25 °C and 50% RH with a loading rate of 20 mm min-1. The tested Silk-Ca ICs were in a rectangular shape with a length of 10 mm and a width of 2 mm and a thickness of 1 mm. Multiple samples ( $\geq 3$ ) were tested for each condition.

Electrochromic device fabrication and measurement. An electrochromic device consisted of an electrochromic layer, transparent electrode, and electrolyte was prepared. Briefly, the cobalt hydroxide thin film, which worked as an electrochromic layer, was deposited on an indium tin oxide (ITO, 20\*10\*0.7 mm) transparent electrode by cathodic electrodeposition. Spin coating was employed to apply the Silk-Ca ICs (Silk-Ca-1-60 wt%. on top of the electrochromic layer as the electrolyte. Typically, the spin-coating process was conducted at a speed of 500 rpm for 5 s, and following 3000 rpm for 40 s. After prepared the device, a potentiostat (Admiral Squidstat Plus) was used to apply the different potentials. The time-dependent transmittance test was carried out by the synchronization of a potentiostat and an Ultraviolet-visible (UV-Vis) spectrophotometry (UV3600Plus, Shimadzu).

**Electrical measurement.** To further identify the flexible and self-healing feature of the conductive Silk-Ca ICs. An electric circuit consisted of LEDs (blue and white color, at a forward voltage of 2.2-2.3 V), Silk-Ca ICs as a conductor, and a DC power supply (8 V was set for this work). Copper wires connected the batteries and the Silk-Ca ICs and the LED in a cascade connection.

**Shape flexibility Silk-Ca Ics.** To identify the shape flexibility of as-prepared Silk-Ca ICs, the soft Silk-Ca ICs was molded into different patterns, which are fabricated by silicone rubber.

GAGSGAGAGSGAGAGSGAGAGSGAGAGSGAGAGSGAGAGY. The initial structure was fully extended, constructed by the UCSF Chimera software.<sup>33</sup> Then, using the method of temperature intervals with the global exchange of replicas (TIGER2),<sup>32</sup> replica exchange molecular dynamics (REMD)<sup>31</sup> simulations were performed with the CHARMM36m forcefield<sup>34</sup> and NAMD 2.14<sup>35</sup> to obtain the equilibrium conformation. In the TIGER2 approach, multiple replicas of the same model system are simulated at different temperatures, where the total number of replicas are chosen by the user, independent of the system size. This independence is feasible as the TIGER2 method performs the Monte-Carlo based swaps between replicas only after quenching all replicas to the same baseline temperature. We first performed the implicit TIGER2 method for the representative silk using the Generalized Born implicit solvent (GBIS).<sup>36</sup> Eight replicas were chosen with temperatures exponentially distributed from 270 K to 600 K. The timestep was set to 4 fs, as we partitioned the mass of heavy atoms into the bonded hydrogen atoms.<sup>37</sup> We performed 6,000 cycles of replica swaps, equaling a simulation time of 360 ns for each replica, hence 2.88 µs in total, and the exchange acceptance was based on the Metropolis criterion. Subsequently, using GROMACS analysis tools<sup>38</sup> with root-mean-square deviation (RMSD) of 6 Å, K-means clustering was performed on the structural ensembles from the last 1,000 exchanges at the baseline replica to obtain equilibrated structures. We then explicitly solvated this lowest-energy representative silk structure in a water box with fully periodic boundary conditions. After energy minimization through conjugate gradient algorithm, two equilibration stages were implemented (1 ns NVT simulation followed by 1 ns NPT simulation) with harmonic constraints to alpha carbons and a timestep of 1 fs. Langevin dynamics<sup>39</sup> and Nosé-Hoover Langevin piston<sup>40</sup> were used for temperature and pressure control at 280 K and 1.013 bar. Rigid bonds were used with the

SHAKE algorithm.<sup>41</sup> Particle-mesh Ewald (PME) method was used to calculate long-range electrostatic interactions.<sup>42</sup> Finally, we carried out the TIGER2 hybrid solvent (TIGER2h) with eight exchange replicas and the same settings, starting from the dissolved representative silk after two equilibration stages. We performed 7,000 cycles, i.e. 420 ns of simulation time for each replica and 3.36 µs in total. After using K-means clustering with the same settings, the conformation of representative silk was chosen from the cluster that had the most similar secondary structure contents compared to our experiments. To explore silk-Ca<sup>2+</sup> interactions, we conducted 110 ns MD simulations for Silk-Ca-1 and Silk-Ca-2 with different water contents. Each simulation box contained eight silk chains to avoid side effects due to the periodic boundary conditions, except for Silk-Ca-1-95 wt%. and Silk-Ca-2-95 wt%. with enough large box size. All simulations were conducted three times, and the last 10 ns, containing 1,000 conformational ensembles of each simulation, were used for subsequent analyses.

Ionic conductivity via MD simulations. In MD simulations, the ionic conductivity  $\sigma$  was calculated based on the Nernst-Einstein equation:<sup>43</sup>

$$\sigma = \frac{q_+^2 \rho_+ D_+}{kT} + \frac{q_-^2 \rho_- D_-}{kT}$$

Where q is the point charge of the ion,  $\rho$  is the number density of the ion, D is the self-diffusion coefficient of the ion, k is the Boltzmann constant, and T is the temperature. The subscript + and – denote cation and anion, respectively. D can be calculated by fitting a linear model to the particle-averaged mean squared displacement (MSD) function with time t, based on the formula:

Where the system contains N particles and x\_j^i (t) denotes the j coordinate of i^th particle at time t.

$$MSD = \frac{1}{N} \sum_{i=0}^{N} \sum_{j=1}^{3} |x_j^i(t) - x_j^i(0)|^2 = 6Dt$$

#### ASSOCIATED CONTENT

## **Supporting Information**

The following files are available free of charge.

Figure S1: rheology results of Silk-Ca-2 Ics at different water contents. Figure S2: DSC results of Silk-Ca powders. Figure S3: ATR-FTIR results of Silk-Ca powders. Figure S4: schematic illustration of Silk-Ca<sup>2+</sup> interaction. Figre S5: SEM results of Silk-Ca powders. Figure S6-S9: ionic conductivity of Silk-Ca ICs. Figure S10-S11 and Table S1-S2: molecular simulation of Silk-Ca ICs. Figure S12: molecular weight of silk fibroin.

#### **AUTHOR INFORMATION**

## **Corresponding Authors**

Jingjie Yeo - Sibley School of Mechanical and Aerospace Engineering, Cornell University, Ithaca, NY 14853, USA; Email: jingjieyeo@cornell.edu

Qiyang Lu - School of Engineering, Westlake University, Hangzhou 310024, China; Key
Laboratory of Precise Synthesis of Functional Molecules of Zhejiang Province,
Instrumentation and Service Centre for Molecular Sciences, Westlake University, Hangzhou
310024, China; Email: <a href="mailto:luqiyang@westlake.edu.cn">luqiyang@westlake.edu.cn</a>

Chengchen Guo - School of Engineering, Westlake University, Hangzhou 310024, China; Email: <a href="mailto:guochengchen@westlake.edu.cn">guochengchen@westlake.edu.cn</a>

## **Authors**

Xin Yu - School of Engineering, Westlake University, Hangzhou 310024, China

Yang Hu - School of Engineering, Westlake University, Hangzhou 310024, China

Haoyuan Shi - Sibley School of Mechanical and Aerospace Engineering, Cornell University,

Ithaca, NY 14853, USA

Ziyang Sun - School of Engineering, Westlake University, Hangzhou 310024, China

Jinghang Li - School of Engineering, Westlake University, Hangzhou 310024, China

Haoran Liu - School of Engineering, Westlake University, Hangzhou 310024, China

Hao Lyu - School of Engineering, Westlake University, Hangzhou 310024, China

Jiujie Xia - School of Engineering, Westlake University, Hangzhou 310024, China

Jingda Meng - School of Engineering, Westlake University, Hangzhou 310024, China

Ruochuan Huang - School of Engineering, Westlake University, Hangzhou 310024, China

Xingyu Lu - Key Laboratory of Precise Synthesis of Functional Molecules of Zhejiang

Province, Instrumentation and Service Centre for Molecular Sciences, Westlake University, Hangzhou 310024, China

## **Author Contributions**

X. Y, Y. H. and H. S. contributed equally to this work. J.Y., Q.L., and C.G. conceived the original idea and designed the experimental protocols with the help of X.Y., Y.H., H.S.; X.Y. performed the experiments and analyses for the soft ionic conductors (thermal analysis, XRD, NMR); Y.H. conducted the ionic conductivity measurement and fabricated the devices. H.S. performed the molecular dynamics simulations and discussed the results. Z.S. and X.L. performed the NMR measurements and data analyses. R.H. assisted with the molecular weight determination. H.L. assisted with the illustration design and drawing. J. L., J.X., and J.M. helped with the preparation of silk fibroin solution and silk-ca powder. J.Y., Q.L., and C.G. supervised the project, revised the manuscript, and provided the funding support. All authors reviewed the manuscript.

## Notes

The authors declare no competing interests.

#### **ACKNOWLEDGMENTS**

This work was supported by foundation of Westlake, National Natural Science Foundation of China (No. 52103129), foundation of Westlake Multidisciplinary Research Initiative Center (No. MRIC20210203). X.Y. acknowledges support from the 2021 Selected Funding Program for the Zhejiang Province Postdoctoral Research Projects. J.Y. acknowledges support provided by the XSEDE program (Grant TG-BIO210063), the US National Science Foundation (Grant No. 2038057) and Cornell University's faculty startup grant. X.Y., Y.H., and H.S. contributed equally to this work.

### References

- [1] Yang, C.; Suo, Z. G. Hydrogel Ionotronics *Nat. Rev. Mater.* **2020**, *3* (6), 125.
- [2] Lei, Z.; Wu, P. Y. Bioinspired Quasi-Solid Ionic Conductors: Materials, Processing, and Applications. *Acc. Mater. Res.* **2021**, *2* (12), 1203.
- [3] Keplinger, C.; Sun, J. Y.; Foo, C. C.; Rothemund, P.; Whitesides, G. M.; Suo, Z. G. Stretchable, Transparent, Ionic Conductors. *Science* **2013**, *341* (6149), 984.
- [4] Liu, Y. Q.; He, K.; Chen, G.; Leow, W. R.; Chen, X. D. Nature-inspired Structural Materials for Flexible Electronic Devices. *Chem. Rev.* **2017**, *117* (6149), 12893.
- [5] Yiming, B.; Han, Y.; Han, Z.L.; Zhang, X. N.; Li, Y., Lian; W.Z., Zhang, M.Q., Yin, J., Sun, T.L., Wu, Z. L. A Mechanically Robust and Versatile Liquid-Free Ionic Conductive Elastomer. *Adv. Mater.* **2021**, *33* (11), 2006111.
- [6] Zhou, Y.; Wan, C. J.; Yang, Y. S.; Yang, H.; Wang, S. C.; Dai, Z. D.; Ji, K. J.; Jiang, H.; Chen, X. D.; Long, Y. Highly Stretchable, Elastic, and Ionic Conductive Hydrogel for Artificial Soft Electronics. *Adv. Funct. Mater.* **2019**, *29* (1), 1806220.
- [7] Cao, Y.; Morrissey, T. G.; Acome, E.; Allec, S. I.; Wong, B. M.; Keplinger, C.; Wang, C. A Transparent, Self-healing, Highly Stretchable Ionic Conductor. *Adv. Mater.* **2017**, *29* (10), 1605099.
- [8] Kim, C. C.; Lee, H. H.; Oh, K. H.; Sun, J. Y. Highly Stretchable, Transparent Ionic Touch Panel. *Science* **2016**, *353* (6300), 682.
- [9] Yang, C. H.; Chen, B.; Zhou, J.; Chen, Y. M.; Suo, Z. G. Electroluminescence of Giant Stretchability. *Adv. Mater.* **2016**, *28* (22), 4480.
- [10] Parida, K.; Kumar, V.; Jiangxin, W.; Bhavanasi, V.; Bendi, R.; Lee, P. S. Highly Transparent, Stretchable, and Self-Healing Ionic-Skin Triboelectric Nanogenerators for Energy Harvesting and Touch Applications. *Adv. Mater.* **2017**, *29* (37), 1702181.
- [11] Liu, J.; Chen, Q.; Liu, Q.; Zhao, B.; Ling, S.; Yao, J.; Shao, Z. Z.; Chen, X. Intelligent Silk Fibroin Ionotronic Skin for Temperature Sensing. *Adv. Mater. Technol.* **2020**, *5* (7), 2000430.

- [12] Liu, Q.; Yang, S.; Ren, J.; Ling, S. J. ACS Mater. Lett. 2020, 2 (7), 7
- [13] Wang, C.Y.; Xia, K. L.; Zhang, Y. Y.; Kaplan, D. L. Silk-based Advanced Materials for Soft Electronics. *Acc. Chem. Res.* **2019**, *52* (10), 2916.
- [14]Zhu, B.W.; Wang, H.; Leow, W. R.; Cai, Y. R.; Loh, X. J.; Han, M. Y.; Chen, X. D. Silk Fibroin for Flexible Electronic Devices. *Adv. Mater.* **2016**, *28* (22), 4250.
- [15] Chen, G.; Matsuhisa, N.; Liu, Z.Y.; Qi, D. P.; Cai, P. Q.; Jiang, Y.; Wan, C. J.; Cui, Y. J.; Leow, W. R.; Liu, Z. J.; Gong, S. Plasticizing Silk Protein for On-Skin Stretchable Electrodes. *Adv. Mater.* **2018**, *30* (21), 1800129.
- [16] Hou, C.; Xu, Z. J.; Qiu, W.; Wu, R. H.; Wang, Y. N.; Xu, Q. C.; Liu, X. Y.; Guo, W. X. A Biodegradable and Stretchable Protein-Based Sensor as Artificial Electronic Skin for Human Motion Detection. *Small* **2019**, *15* (11), 1805084.
- [17] Ling, S. J.; Wang, Q.; Zhang, D.; Zhang, Y. Y.; Mu, X.; Kaplan, D. L.; Buehler, M. J. Integration of Stiff Graphene and Tough Silk for the Design and Fabrication of Versatile Electronic Materials. *Adv. Funct. Mater.* **2018**, *28* (9), 1705291.
- [18] Liu, H. T.; Wei, W.; Zhang, L.; Xiao, J. L.; Pan, J.; Wu, Q.; Ma, S. Q.; Dong, H.; Yu, L.T.; Yang, W. Z. Shape-Engineerable Silk Fibroin Papers for Ideal Substrate Alternatives of Plastic Electronics. *Adv. Funct. Mater.* **2021**, *31* (52), 2104088.
- [19] Seo, J.W.; Kim, H. J.; Kim, K. H.; Choi, S. Q.; Lee, H. J. Calcium-Modified Silk as a Biocompatible and Strong Adhesive for Epidermal Electronics. *Adv. Funct. Mater.* **2018**, *28* (36), 1800802.
- [20] Wang, Q.; Ling, S. J.; Liang, X. P.; Wang, H. M.; Lu, H. J.; Zhang, Y. Y. Self-Healable Multifunctional Electronic Tattoos Based on Silk and Graphene. *Adv. Funct. Mater.* **2019**, *29* (16), 1808695.
- [21] Jia, Z. R.; Gong, J. L.; Zeng, Y.; Ran, J.; Liu, J. H.; Wang, K. F.; Xie, C. M.; Lu, X.; Wang, J. Bioinspired Conductive Silk Microfiber Integrated Bioelectronic for Diagnosis and Wound Healing in Diabetes. Adv. Funct. Mater. **2021**, *31* (19), 2010461.

[22] Huang, W. W.; Ling, S. J.; Li, C. M.; Omenetto, F. G.; Kaplan, D. L. Silkworm Silk-based Materials and Devices Generated Using Bio-nanotechnology. *Chem. Soc. Rev.* **2018**, *47* (17), 6486.

[23] Koh, L. D.; Cheng, Y.; Teng, C. P.; Khin, Y. W.; Loh, X. J.; Tee, S. Y.; Low, M.; Ye, E.; Yu, H. D.; Zhang, Y. W.; Han, M. R. Structures, Mechanical Properties and Applications of Silk Fibroin Materials. *Prog. Polym. Sci.* **2015**, *46*, 86.

[24] Zhao, B. H.; Chen, Q. Y.; Da, G. H.; Yao, J. R.; Shao, Z. Z.; Chen, X. A Highly Stretchable and Anti-freezing Silk-based Conductive Hydrogel for Application as a Self-adhesive and Transparent Ionotronic Skin. *J. Mater. Chem. C* **2021**, *9* (28), 8955.

[25] Cao, L. T.; Liu, Q.; Ren, J.; Chen, W. S.; Pei, Y.; Kaplan, D. L.; Ling, S. J. Electro-Blown Spun Silk/Graphene Nanoionotronic Skin for Multifunctional Fire Protection and Alarm. *Adv, Mater.* **2021**, *33* (38), 2102500.

[26] Chen, Q. Y.; Tang, H.; Liu, J. L; Wang, R. R.; Sun, J.; Yao, J. R.; Shao, Z. Z.; Chen, X. Silk-based Pressure/Temperature Sensing Bimodal Ionotronic Skin with Stimulus Discriminability and Low Temperature Workability. *Chem. Eng. J.* **2021**, *422*, 130091.

[27]He, F. L.; You, X. Y.; Gong, H.; Yang, Y.; Bai, T.; Wang, W. G.; Guo, W. X.; Liu, X. Y.; Ye, M. D. Stretchable, Biocompatible, and Multifunctional Silk Fibroin-based Hydrogels Toward Wearable Strain/Pressure Sensors and Triboelectric Nanogenerators., *ACS. Appl. Mater. Inter.* **2020**, *12* (5), 6442.

[28] Yang, S.; Liu, Q.; Ren, J.; Ling, S. J. Influence of Hydrated Protons on Temperature and Humidity Rsponsiveness of Silk Fibroin Hydrogel Ionotronics. *Giant* **2021**, *5*, 100044.

[29] Guo, C. C.; Li, C. M.; Vu, H. V.; Hanna, P.; Lechtig, A.; Qiu, Y. M.; Mu, X.; Ling, S. J.; Nazarian, A.; Lin, S. J.; Kaplan D. L. Thermoplastic Moulding of Regenerated Silk. *Nat. Mater.* **2020**, *19* (1), 102.

- [30] Ye, Y. H.; Zhang, Y. F.; Chen, Y.; Han, X. S.; Jiang, F. Cellulose Nanofibrils Enhanced, Strong, Stretchable, Freezing-tolerant Ionic Conductive Organohydrogel for Multi-functional Sensors. *Adv. Funct. Mater.* **2020**, *30* (35), 2003430.
- [31] Sugita, Y.; Okamoto, Y. Replica-exchange Molecular Dynamics Method for Protein Folding. *Chem. Phys. Lett.* **1999**, *314* (1-2), 141.
- [32] Geist, N.; Kulke, M.; Schulig, L.; Link, A.; Langel, W. Replica-based Protein Structure Sampling Methods II: Advanced Hybrid Solvent TIGER2hs. *J. Phys. Chem. B* **2019**, *123* (28), 5995.
- [33] Pettersen, E. F.; Goddard, T. D.; Huang, C. C.; Couch, G. S.; Greenblatt, D. M.; Meng, E.C.; Ferrin, T. E. UCSF Chimera-a Visualization System for Exploratory Research and Analysis. *J. Comput. Chem.* **2004**, *25* (13), 1605.
- [34] Huang, J.; Rauscher, S.; Nawrocki, G.; Ran, T.; Feig, M.; De Groot, B. L.; Grubmüller, H.; MacKerell, A. D. CHARMM36m: An Improved Force Field for Folded and Intrinsically Disordered Proteins. *Nat. Methods* **2017**, *14* (1), 71.
- [35] Phillips, J. C.; Hardy, D. J.; Maia, J. D.; Stone, J. E.; Ribeiro, J. V.; Bernardi, R. C.; Buch, R.; Fiorin, G.; Hénin, J.; Jiang, W. Scalable Molecular Dynamics on CPU and GPU Architectures with NAMD. *J. Chem. Phys.* **2020**, *153* (4), 044130.
- [36] Still, W. C.; Tempczyk, A.; Hawley, R. C.; Hendrickson, T. Semianalytical Treatment of Solvation for Molecular Mechanics and Dynamics. *J. Am. Chem. Soc.* **1990,** *112* (16), 6127.
- [37] Hopkins, C. W.; Le Grand, S.; Walker, R. C.; Roitberg, A. E. Long-time-step Molecular Dynamics through Hydrogen Mass Repartitioning. *J. Chem. Theory Comput.* **2015**, *11* (4), 1864.
- [38] Abraham, M. J.; Murtola, T.; Schulz, R.; Páll, S.; Smith, J. C.; Hess, B.; Lindahl, E. GROMACS: High Performance Molecular Simulations through Multi-level Parallelism from Laptops to Supercomputers. *SoftwareX* **2015**, *1*, 19.

[39] Phillips, J. C.; Braun, R.; Wang, W.; Gumbart, J.; Tajkhorshid, E.; Villa, E.; Chipot, C.; Skeel, R. D.; Kale, L.; Schulten, K. Scalable Molecular Dynamics with NAMD. *J. Comput. Chem.* **2005**, *26* (16), 1781.

[40] Feller, S. E.; Zhang, Y.; Pastor, R. W.; Brooks, B. R. Constant Pressure Molecular Dynamics Simulation: The Langevin Piston Method. *J. Chem. Phys.* **1995**, *103* (11), 4613.

[41] Kräutler, V.; Van Gunsteren, W. F.; Hünenberger, P. H. A Fast SHAKE Algorithm to Solve Distance Constraint Equations for Small Molecules in Molecular Dynamics Simulations. *J. Comput. Chem.* **2001**, *22* (5), 501.

[42] Essmann, U.; Perera, L.; Berkowitz, M. L.; Darden, T.; Lee, H.; Pedersen, L. G. A Smooth Particle Mesh Ewald Method. *J. Chem. Phys.* **1995**, *103* (11), 8577.

[43] Yllö, A.; Zhang, C. Experimental and Molecular Dynamics Study of the Ionic Conductivity in Aqueous LiCl Electrolytes. *Chem. Phys. Lett.* **2019**, 729, 6.

## **Table of Content**

